Acta Crystallographica Section D
Biological Crystallography
ISSN 0907-4449

Inhibitor-bound structures of human pyruvate dehydrogenase kinase 4

Mutsuko Kukimoto-Niino,[a]‡ Alexander Tokmakov,[a]‡§ Takaho Terada,[a] Naomi Ohbayashi,[a] Takako Fujimoto,[a] Sumiko Gomi,[a] Ikuya Shiromizu,[b] Masaki Kawamoto,[b] Tomokazu Matsusue,[b] Mikako Shirouzu[a] and Shigeyuki Yokoyama[a,c]*

[a]RIKEN Systems and Structural Biology Center, 1-7-22 Suehiro-cho, Tsurumi-ku, Yokohama 230-0045, Japan, [b]Discovery Research, Mochida Pharmaceutical Co. Ltd, 722 Uenohara, Jimba, Gotemba, Shizuoka 412-8524, Japan, and [c]Department of Biophysics and Biochemistry, Graduate School of Science, The University of Tokyo, Bunkyo-ku, Tokyo 113-0033, Japan

‡ These authors contributed equally to this work.
§ Present address: Research Center for Environmental Genomics, Kobe University, Nada 657-8501, Japan.

Correspondence e-mail: yokoyama@biochem.s.u-tokyo.ac.jp

Received 14 January 2011
Accepted 20 June 2011

PDB References:
PDK4–AMPPNP, 2e0a;
PDK4–M77976, 2zdx;
PDK4–ADP, 2zdy.

The mitochondrial pyruvate dehydrogenase complex (PDC) catalyzes the oxidative decarboxylation of pyruvate to acetyl-CoA. PDC activity is tightly regulated by four members of a family of pyruvate dehydrogenase kinase isoforms (PDK1–4), which phosphorylate and inactivate PDC. Recently, the development of specific inhibitors of PDK4 has become an especially important focus for the pharmaceutical management of diabetes and obesity. In this study, crystal structures of human PDK4 complexed with either AMPPNP, ADP or the inhibitor M77976 were determined. ADP-bound PDK4 has a slightly wider active-site cleft and a more disordered ATP lid compared with AMPPNP-bound PDK4, although both forms of PDK4 assume open conformations with a wider active-site cleft than that in the closed conformation of the previously reported ADP-bound PDK2 structure. M77976 binds to the ATP-binding pocket of PDK4 and causes local conformational changes with complete disordering of the ATP lid. M77976 binding also leads to a large domain rearrangement that further expands the active-site cleft of PDK4 compared with the ADP- and AMPPNP-bound forms. Biochemical analyses revealed that M77976 inhibits PDK4 with increased potency compared with the previously characterized PDK inhibitor radicicol. Thus, the present structures demonstrate for the first time the flexible and dynamic aspects of PDK4 in the open conformation and provide a basis for the development of novel inhibitors targeting the nucleotide-binding pocket of PDK4.

1. Introduction

The mitochondrial pyruvate dehydrogenase complex (PDC) plays a key role in glucose metabolism by catalyzing the oxidative decarboxylation of pyruvate and thereby providing acetyl-CoA and NADH for the tricarboxylic acid cycle and lipid biosynthesis. PDC is composed of multiple copies of four components: pyruvate dehydrogenase (E1), dihydrolipoamide acetyltransferase (E2), dihydrolipoamide dehydrogenase (E3) and E3-binding protein (E3BP) (Patel & Roche, 1990). Two associated enzymes, inactivating pyruvate dehydrogenase kinase (PDK) and activating pyruvate dehydrogenase phosphatase (PDP), control PDC activity by the reversible phosphorylation of three serine residues in the E1 component of PDC (Holness & Sugden, 2003; Patel & Korotchkina, 2006). PDK must bind to the E2 inner lipoyl (L2) domain for its catalytic function (Ono *et al.*, 1993; Liu *et al.*, 1995; Tuganova *et al.*, 2002; Roche *et al.*, 2003).

There are four mammalian members (PDK1–4) of the PDK isoform family (Popov *et al.*, 1993; Gudi *et al.*, 1995; Rowles *et al.*, 1996). They display different tissue distributions,

Table 1
X-ray data-collection and refinement statistics.

Values in parentheses are for the outer shell.

	PDK4–AMPPNP	PDK4–ADP	PDK4–M77976
Data collection			
Space group	$P2_1$	$P2_1$	$P2_1$
Unit-cell parameters			
a (Å)	71.1	70.7	68.1
b (Å)	68.5	69.1	69.1
c (Å)	79.8	81.5	85.6
β (°)	101.1	99.7	99.7
Wavelength (Å)	1.0	1.0	1.0
Resolution range (Å)	50–1.85 (1.92–1.85)	50–2.40 (2.49–2.40)	50–2.53 (2.62–2.53)
Unique reflections	63193	30416	23666
Multiplicity	3.2	3.5	2.9
Completeness (%)	99.6 (99.8)	99.8 (100)	91.1 (94.1)
$\langle I/\sigma(I)\rangle$	32.2 (3.1)	26.4 (6.2)	24.8 (3.2)
$R_{\rm merge}$†	0.035 (0.365)	0.047 (0.214)	0.041 (0.326)
Refinement			
Resolution range (Å)	26.67–1.86	26.78–2.40	48.68–2.54
No. of reflections	63176	28142	22738
No. of atoms			
Protein	5704	5697	5500
Ligand/ion	64	71	44
Water	311	180	79
R factor/free R factor‡	0.196/0.231	0.190/0.245	0.222/0.290
R.m.s.d. bond lengths (Å)	0.008	0.005	0.006
R.m.s.d. bond angles (°)	1.4	0.8	0.9
Ramachandran plot			
Most favoured regions (%)	93.2	93.0	90.3
Additional allowed regions (%)	6.7	6.9	9.3
Generously allowed regions (%)	0.2	0.2	0.3
Disallowed regions (%)	0.0	0.0	0.0

† $R_{\rm merge} = \sum_{hkl}\sum_i |I_i(hkl) - \langle I(hkl)\rangle| / \sum_{hkl}\sum_i I_i(hkl)$, where $I_i(hkl)$ is the observed intensity and $\langle I(hkl)\rangle$ is the average intensity. ‡ The free R factor is calculated for 10% of randomly selected reflections excluded from refinement.

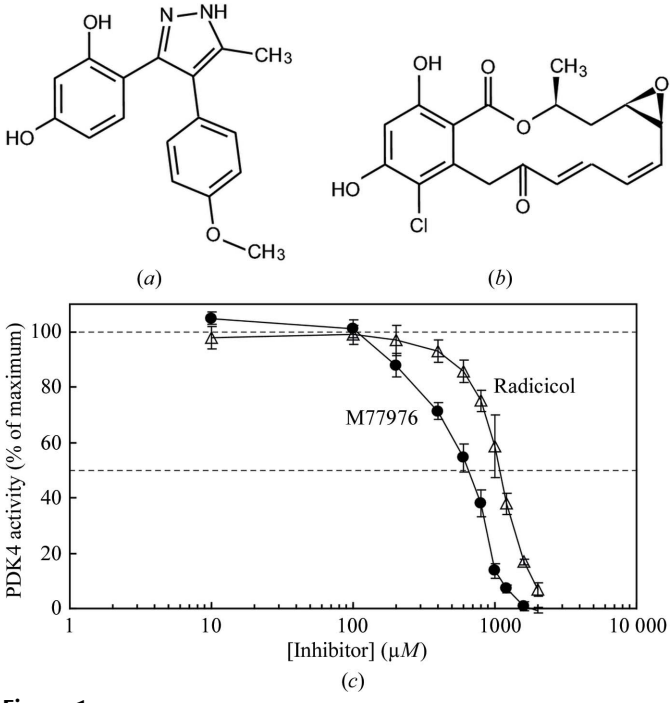

Figure 1
Chemical structures of (*a*) M77976 and (*b*) radicicol. (*c*) Inhibition of PDK4 by increasing concentrations of M77976 (closed circles) and radicicol (open triangles). IC_{50} estimates are quoted in the text. The PDK4 activities in the absence of inhibitors are set to 100. Error bars indicate standard deviations (n = 4).

phosphorylation-site specificities and binding affinities for the L2 domain (Bowker-Kinley *et al.*, 1998; Korotchkina & Patel, 2001; Tuganova *et al.*, 2002). PDK4 appears to be especially important for maintaining glucose homeostasis (Holness & Sugden, 2003) and is selectively upregulated in most tissues in response to starvation and hormonal imbalance, such as insulin resistance and diabetes (Wu *et al.*, 1998; Sugden & Holness, 2002). Therefore, PDK4 is recognized as a potential therapeutic target for the treatment of obesity and diabetes.

The PDKs, together with the related branched-chain α-ketoacid dehydrogenase kinase (BCK), constitute a distinct group of mitochondrial protein kinases that lack the characteristic sequence motifs of eukaryotic protein kinases (Popov *et al.*, 1993; Harris *et al.*, 1995; Bowker-Kinley & Popov, 1999). Crystal structures of rat PDK2 and BCK and of the four human PDK isoforms have been solved (Steussy *et al.*, 2001; Machius *et al.*, 2001; Kato *et al.*, 2005, 2007; Knoechel *et al.*, 2006; Wynn *et al.*, 2008). They share a common dimeric structure, with two identical subunits each consisting of a C-terminal nucleotide-binding domain and an N-terminal regulatory domain. The C-terminal domain, which provides a large dimer interface, has the unique ATP-binding fold common to the GHKL (gyrase, Hsp90, histidine kinase and MutL) ATPase/kinase superfamily of proteins (Dutta & Inouye, 2000). The fold is an α/β sandwich consisting of a four-stranded mixed β-sheet and three α-helices. The four conserved motifs (N and G1–3 boxes) and the flexible loop, termed the ATP lid, constitute the nucleotide-binding site. The N-terminal domain is dominated by a four-helix bundle structure. It contains several distinct allosteric sites (Knoechel *et al.*, 2006), including the lipoyl-binding pocket (Kato *et al.*, 2005).

In the human PDK3–L2 and rat PDK2–L2 complexes the C-terminal tail contributes to dimer formation by interacting with the N-terminal domain of the other subunit (Kato *et al.*, 2005; Green *et al.*, 2008). Thus, the C-terminal tails of the two subunits assume a crossover configuration designated the 'cross arms' (Kato *et al.*, 2005). The binding of L2 or synthetic ligands such as Nov3r, AZ12 and AZD7545 to the N-terminal domain promotes the cross-arms formation, which stabilizes open conformations of PDK1–3 with wider active-site clefts (Kato *et al.*, 2005, 2007; Knoechel *et al.*, 2006; Green *et al.*, 2008) compared with the closed conformation of rat PDK2 with completely disordered C-terminal tails (Steussy *et al.*, 2001). On the other hand, the PDK4 structure is unique in that it adopts an intrinsically open conformation without L2

binding, which accounts for its unique biochemical properties (Wynn *et al.*, 2008). The authors showed that unlike PDK1–3, PDK4 possesses high basal activity and is hardly activated by L2, which is related to its low L2-binding affinity.

Determination of the inhibitor-bound structure of PDK4 is especially important for pharmaceutical purposes and for understanding the isoform-specific regulation of PDK. In this study, we determined the 2.54 Å resolution crystal structure of

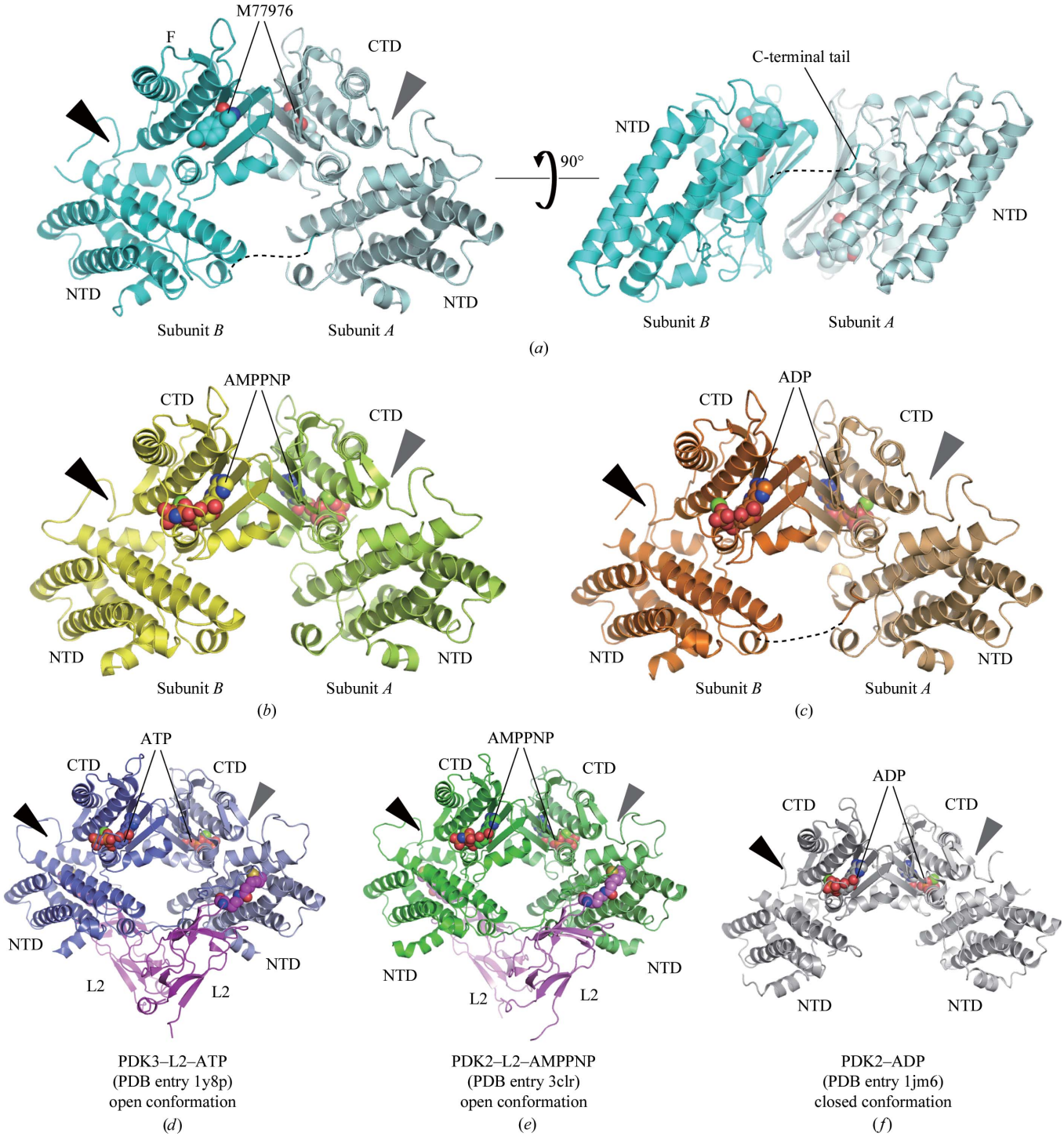

Figure 2
Crystal structures of human PDK4 and comparison with other PDK structures. Ribbon representations of the (*a*) PDK4–M77976 (subunit *A*, pale cyan; subunit *B*, dark cyan), (*b*) PDK4–AMPPNP (subunit *A*, lime green; subunit *B*, yellow) and (*c*) PDK4–ADP (subunit *A*, wheat; subunit *B*, orange) dimer structures. The partially ordered regions in the C-terminal tails of PDK4–M77976 and PDK4–ADP are linked by dashed lines. Ribbon representations are shown of the previously reported (*d*) human PDK3–L2–ATP (blue), (*e*) rat PDK2–L2–AMPPNP (green) and (*f*) rat PDK2–ADP (grey) structures. The L2 domains are coloured magenta. NTD and CTD denote the N-terminal and C-terminal domains, respectively. The arrowhead indicates the active-site cleft. M77976, AMPPNP, ADP, ATP, the magnesium ion and the lipoyl group of L2 are shown as sphere models.

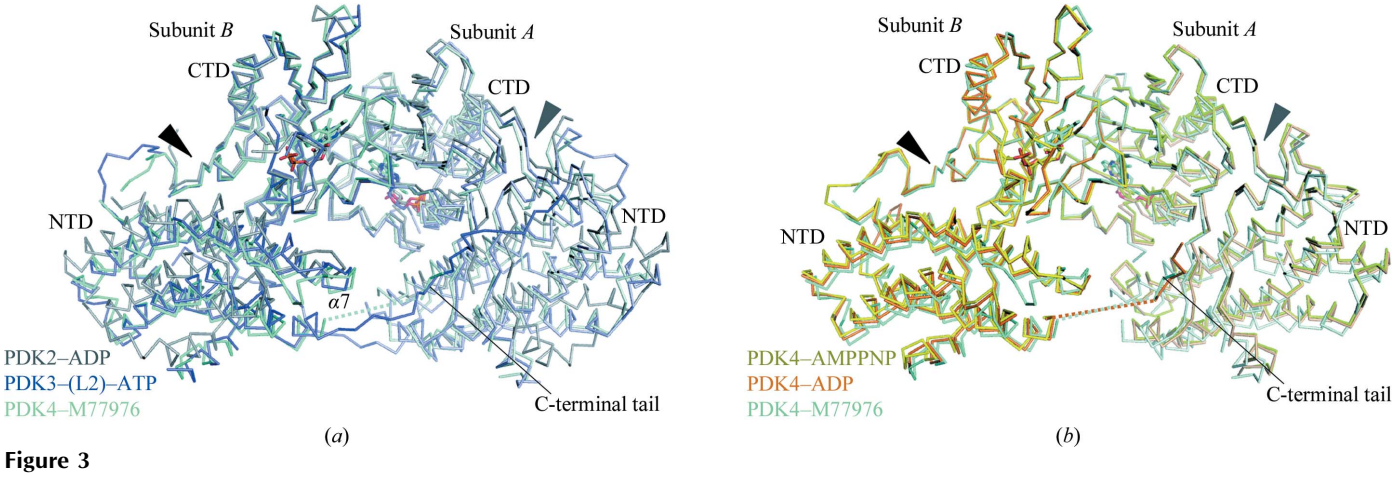

Figure 3
(*a*) Superposition of the C$^{\alpha}$ atoms of the previously reported rat PDK2–ADP in the closed conformation and human PDK3–L2–ATP in the open conformation on those of human PDK4–M77976 determined in this study. The L2 domains bound to PDK3 are omitted from this figure. (*b*) Superposition of the C$^{\alpha}$ atoms of PDK4–M77976 and PDK4–ADP on those of PDK4–AMPPNP. The colouring of the molecules is the same as in Fig. 2. The superposition is based on the C-terminal domain of the left subunit (subunit *B*) of each dimer. NTD and CTD denote the N-terminal and C-terminal domains, respectively. The arrowhead indicates the active-site cleft. Bound ligands are shown as stick models.

human PDK4 in complex with the inhibitor M77976 identified by *in vitro* screening. For direct comparison, the AMPPNP- and ADP-bound structures were also determined at 1.86 and 2.40 Å resolution, respectively. M77976 binding to the ATP-binding pocket of PDK4 causes significant structural changes in the binding site and shifts the relative positions of the N- and C-terminal domains. Comparisons with the previously determined PDK structures revealed that the domain reorganization induced by the ATP-competitive inhibitor is unique to PDK4.

2. Materials and methods

2.1. Protein expression and purification

The DNA encoding residues 20–411 of human PDK4 was cloned into the baculovirus transfer vector pBlueBac4.5 (Invitrogen) as a fusion with an N-terminal His_6 tag and a PreScission protease cleavage site. The baculovirus for His-tagged PDK4 was created using the Bac-N-Blue Baculovirus Expression System (Invitrogen) and was used to infect Sf9 cells.

Cells from a 500 ml Sf9 culture were harvested 48 h after infection, resuspended in 100 ml lysis buffer (20 m*M* Tris–HCl buffer pH 8.0 containing 400 m*M* NaCl, 20 m*M* imidazole, 0.05% Triton X-100, 2 m*M* β-mercaptoethanol and 20% glycerol) and disrupted by sonication. The sample was centrifuged at 16 000*g* at 277 K for 20 min. The supernatant was loaded onto an Ni–

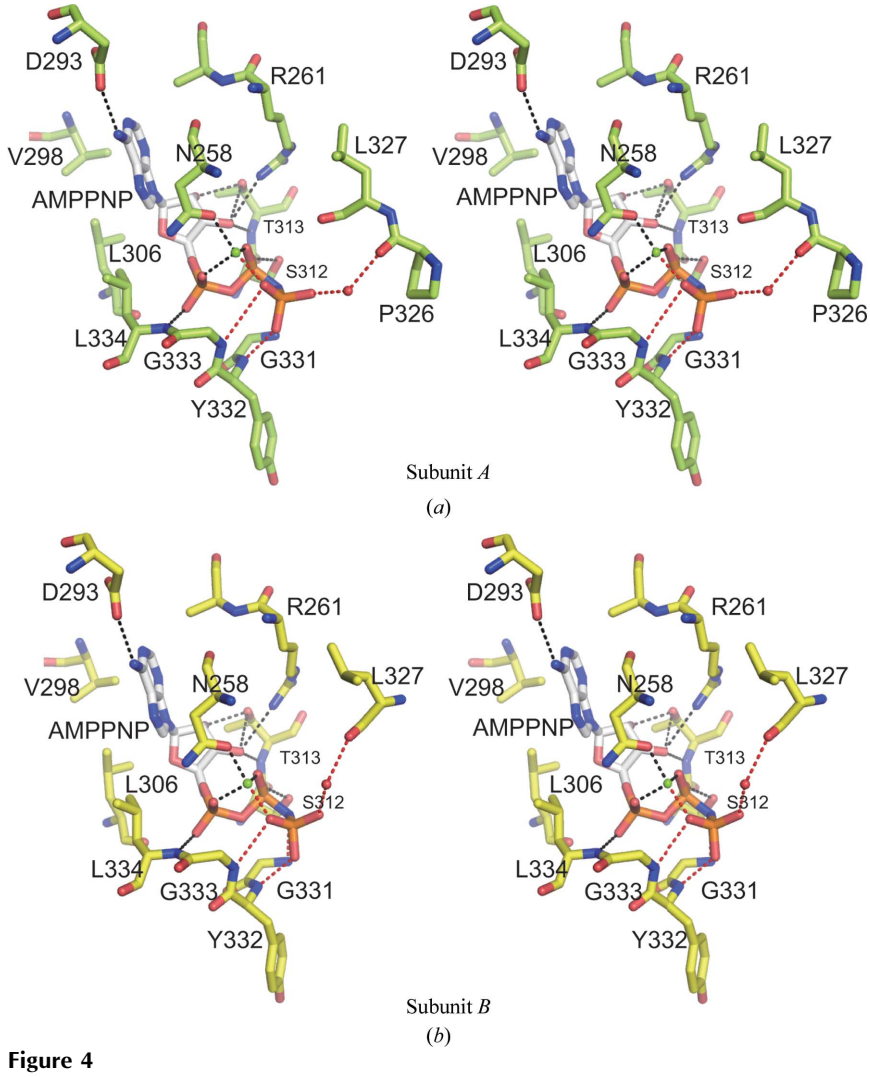

Figure 4
Interactions of PDK4 residues with AMPPNP in (*a*) subunit *A* (lime green) and (*b*) subunit *B* (yellow) (stereoview). AMPPNP is shown as a white-based stick model. The magnesium ions are shown as green dots. Hydrogen bonds are shown by dashed lines and coordinating water molecules are indicated as red dots.

NTA Superflow column (Qiagen) and was eluted with 20 m*M* Tris–HCl buffer pH 8.0 containing 400 m*M* NaCl, 500 m*M* imidazole, 2 m*M* β-mercaptoethanol and 20% glycerol. The His_6 tag was cleaved by PreScission protease (GE Healthcare Biosciences) at 277 K for 16 h. The protease and the cleaved His_6 tag were then removed by passage through GSTrap and HisTrap (GE Healthcare Biosciences) columns, respectively. The protein sample was further purified by ion exchange on a Mono Q 10/100 GL column (GE Healthcare Biosciences) and by size-exclusion chromatography on a HiLoad 16/60 Superdex 75 column (GE Healthcare Biosciences) pre-equilibrated with 20 m*M* Tris–HCl buffer pH 8.0 containing 150 m*M* NaCl, 1 m*M* DTT and 20% glycerol. The protein sample was concentrated to 27.9 mg ml^{-1}. The yield of the purified protein was 2.63 mg per 500 ml cell culture.

2.2. Crystallization and data collection

Prior to crystallization, 10 m*M* $MgCl_2$ and 5 m*M* AMPPNP were added to the protein solution. The crystallization conditions were screened by the 96-well sitting-drop vapour-diffusion method at 293 K. Diffraction-quality crystals of PDK4 complexed with AMPPNP were grown against a reservoir solution consisting of 1.7 *M* ammonium sulfate, 2% PEG 400 and Na HEPES buffer pH 7.1 by the hanging-drop vapour-diffusion method. Crystals of PDK4 complexed with M77976 and ADP were obtained by soaking the PDK4–AMPPNP crystals in 5 m*M* ADP or 1 m*M* M77976. Single crystals were coated with Paratone-N and 10% glycerol, mounted in a nylon loop (Hampton Research) and flash-cooled in the cold stream of the goniometer. All data were collected at a wavelength of 1.0 Å at BL32B2, SPring-8 (Harima) and were recorded on a Jupiter210 CCD detector (Rigaku). The diffraction data were processed with the *HKL-2000* program (Otwinowski & Minor, 1997).

2.3. Structure determination and refinement

The structure of the PDK4–AMPPNP complex was determined by molecular replacement with the program *MOLREP* from *CCP*4 (Winn *et al.*, 2011) using rat PDK2 (PDB entry 1jm6; Steussy *et al.*, 2001) as a search model. The model was corrected iteratively using *O* (Jones *et al.*, 1991) and structure refinement was performed using the *Crystallography & NMR System* (*CNS*; Brünger *et al.*, 1998). The final models of the PDK4–M77976 and PDK4–ADP complexes were generated after several cycles of model building and refinement using *QUANTA* (Accelrys Inc., San Diego, USA) and *CNX*, respectively. Refinement statistics are presented in Table 1. The quality of the model was inspected by the program *PROCHECK* (Laskowski *et al.*, 1993). Structural similarities were calculated with the programs *DALI* (Holm & Sander, 1993) and *LSQKAB* from *CCP*4 (Winn *et al.*, 2011). Graphical figures were created using the program *PyMOL* (DeLano, 2002). The atomic coordinates for the PDK4–AMPPNP, PDK4–M77976 and PDK4–ADP complexes have been deposited in the Protein Data Bank with accession codes 2e0a, 2zdx and 2zdy, respectively.

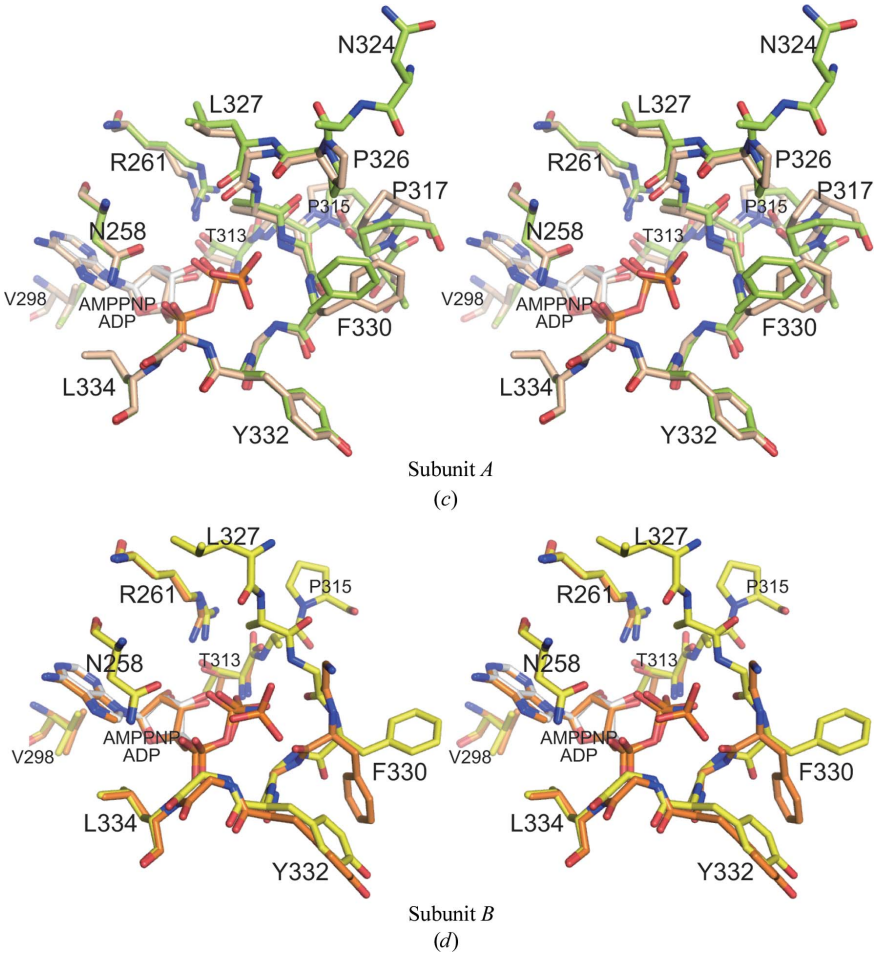

Figure 4 (continued)
The AMPPNP-binding site is superposed onto the ADP-binding site of (*c*) subunit *A* (wheat) and (*d*) subunit *B* (orange) (stereoview). ADP is shown as a (*c*) wheat or (*d*) orange-based stick model.

2.4. *In vitro* inhibition assays

The substrate peptide Ac-YHGHSM-SDPGVSYR was synthesized at the Support Unit for Bio-material Analysis in the RIKEN Brain Science Institute (BSI) Research Resources Center (RRC). Purified PDK4 (0.217 mg ml^{-1}) was incubated with 0.5 m*M* substrate peptide at 303 K for 30 min in a reaction solution (50 µl) consisting of 50 m*M* Tris–HCl pH 8.0, 20 m*M* KH_2PO_4, 0.5 m*M* EDTA, 2 m*M* $MgCl_2$, 30 m*M* KCl, 2 m*M* DTT, 10 m*M* NaF and 200 µ*M* ATP with or without the indicated concentrations of M77976 or radicicol.

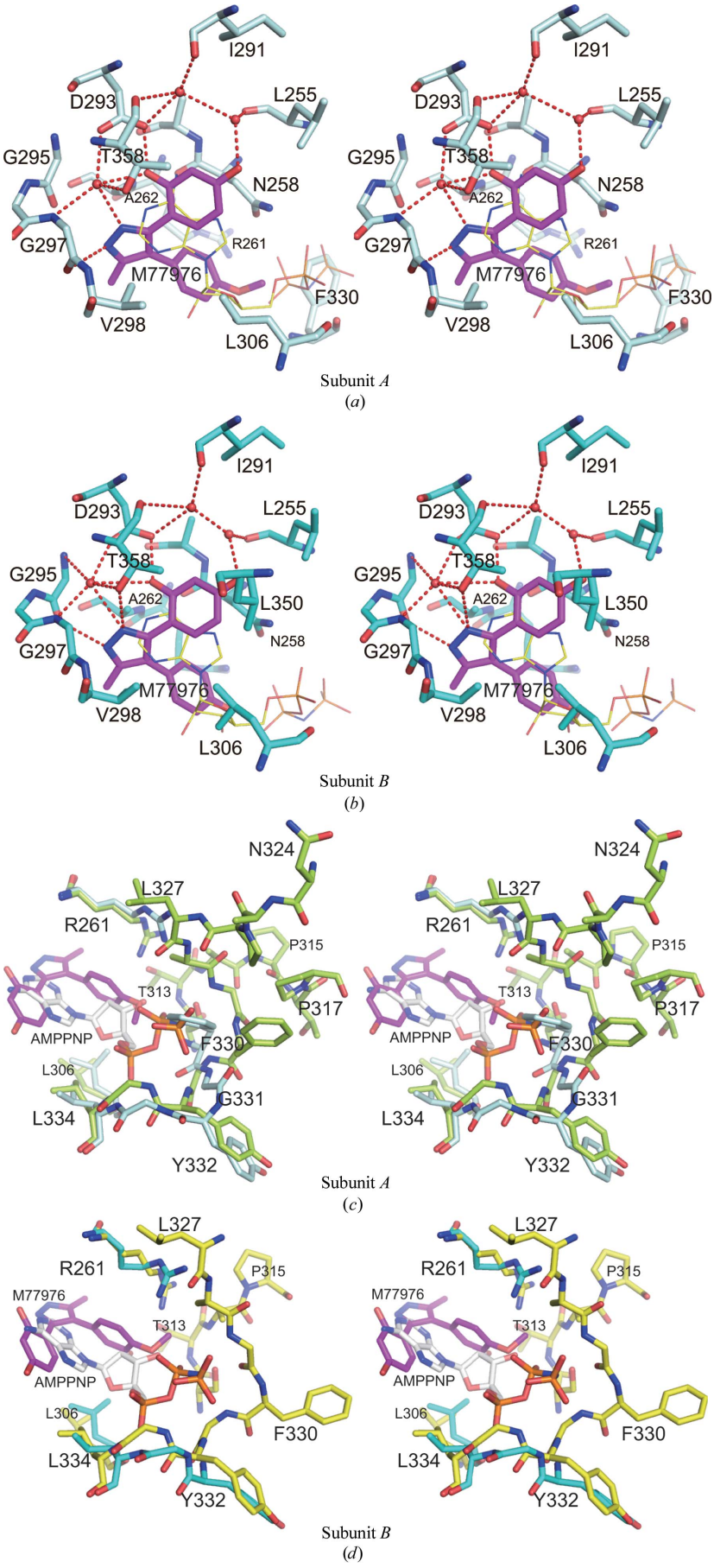

M77976 and radicicol (Sigma–Aldrich) were dissolved in DMSO and added to the reaction solution to a 5% final DMSO concentration. ATP consumption was determined by using a Kinase-Glo Max luminescent kinase assay (Promega) kit, which quantifies the amount of ATP in the reaction solution. Glow-type luminescence was recorded after 30 min using a Fusion universal microplate analyzer (Packard).

3. Results and discussion

3.1. Inhibition of PDK4 by M77976

In our search for compounds that inhibit PDK4 activity, we identified 3-(2,4-dihydroxyphenyl)-4-(4-methoxyphenyl)-5-methyl-1*H*-pyrazole, designated M77976 (Fig. 1*a*). The previously reported PDK inhibitor radicicol also possesses a dihydroxyphenyl ring (Fig. 1*b*) and inhibits kinase activity by directly binding to the ATP-binding pocket of PDK3 (Kato *et al.*, 2007). We therefore performed comparative biochemical analyses of PDK4 activity inhibition by M77976 and radicicol (Fig. 1*c*). Under our assay conditions, the M77976 concentration causing 50% inhibition (IC_{50}) of PDK4 was estimated to be 648 µ*M*. On the other hand, radicicol exhibits a 1.67-fold higher IC_{50} value (1079 µ*M*) compared with M77976. Therefore, M77976 inhibits PDK4 with enhanced potency compared with radicicol.

3.2. Crystal structure determination

We crystallized human PDK4 in the presence of the nonhydrolyzable ATP analog AMPPNP. Soaking the PDK4–AMPPNP crystals with M77976 resulted in the formation of PDK4–M77976 crystals. Similarly, PDK4–ADP crystals were obtained by soaking the PDK4–AMPPNP crystals with ADP. All crystals belonged to the primitive monoclinic space group $P2_1$

Figure 5
Interactions of PDK4 residues with M77976 in (*a*) subunit *A* (pale cyan) and (*b*) subunit *B* (dark cyan) (stereoview). M77976 is shown as a magenta-based model. Hydrogen bonds are shown by red dashed lines and coordinating water molecules are indicated as dots. AMPPNP from PDK4–AMPPNP is shown in yellow-based lines as a guide. The M77976-binding site is superposed onto the AMPPNP-binding site of (*c*) subunit *A* (lime green) and (*d*) subunit *B* (yellow) (stereoview). AMPPNP is shown as white-based stick model.

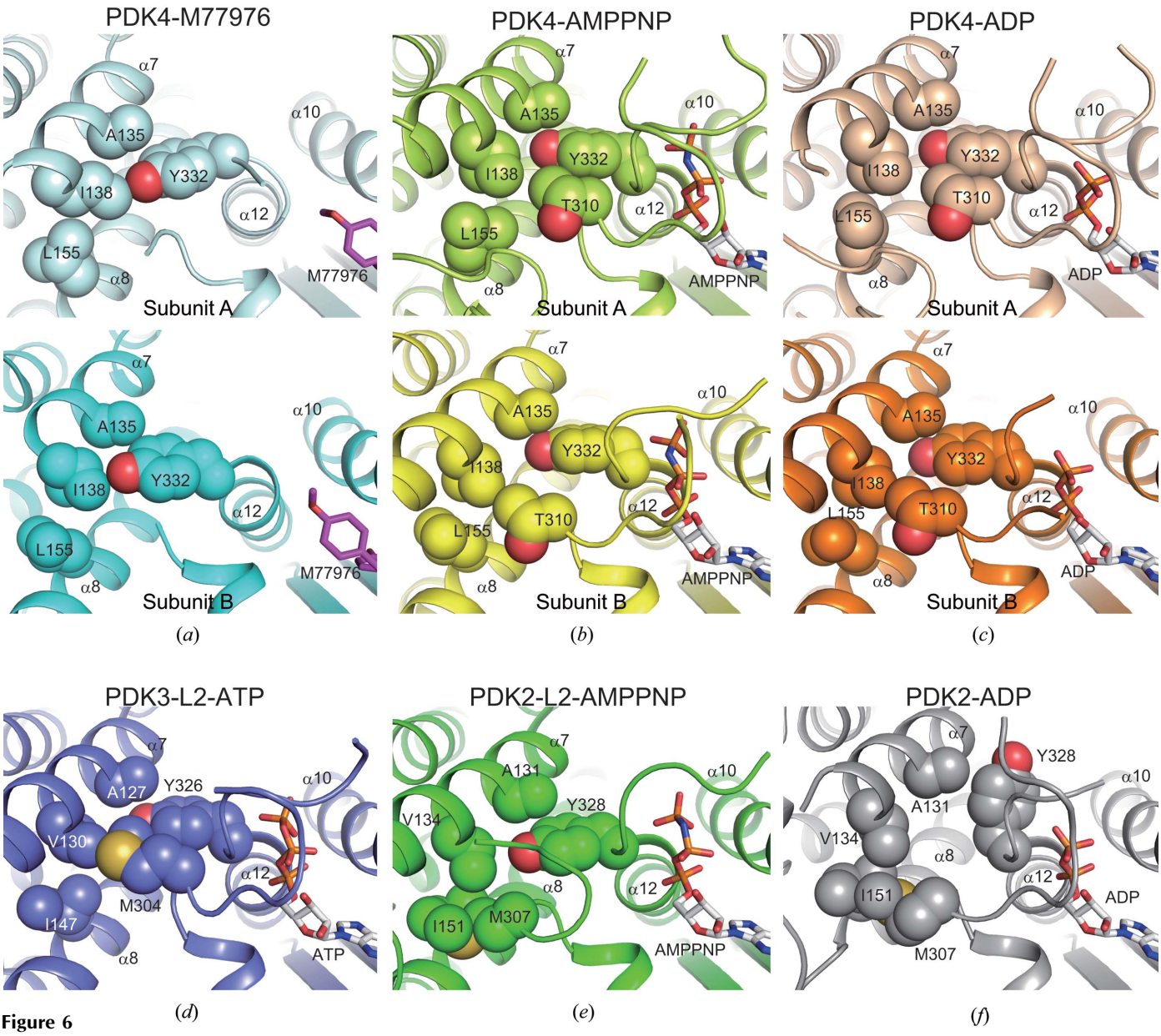

Figure 6
Inter-domain interactions in (*a*) PDK4–M77976, (*b*) PDK4–AMPPNP, (*c*) PDK4–ADP, (*d*) PDK3–L2–ATP, (*e*) rat PDK2–L2–AMPPNP and (*f*) rat PDK2–ADP coloured as in Fig. 2. Selected residues are shown as sphere models and bound ligands are shown as stick models.

and contained one PDK4 dimer per asymmetric unit. The structures of PDK4–AMPPNP, PDK4–ADP and PDK4–M77976 were determined by molecular replacement and refined to 1.86, 2.40 and 2.54 Å resolution, respectively (Table 1). Each structure contained two subunits (*A* and *B*) that form a homodimer with a noncrystallographic symmetry axis (Figs. 2*a*, 2*b* and 2*c*; right and left subunits, respectively). The bound AMPPNP, ADP and M77976 molecules were unambiguously identified in the electron-density map at the nucleotide-binding site in their respective complexes (Supplementary Fig. S1[1]). Therefore, M77976, like AMPPNP and ADP, probably inhibits PDK4 in an ATP-competitive manner.

The PDK4 dimers displayed some asymmetric features. Firstly, α7 and the following α7–α8 loop assume different conformations in the two subunits (Supplementary Fig. S2[1]). Secondly, the ATP lid of subunit *B* is more disordered compared with that of subunit *A* (Supplementary Fig. S2[1]). Thirdly, in PDK4–M77976 and PDK4–ADP the C-terminal residues around the conserved 'DW' motif of subunit *B* (residues 393–398 and residues 394–396, respectively) interact with the N-terminal domain of subunit *A* (Figs. 2*a* and 2*c*), but the corresponding residues of subunit *A* are not well defined owing to their weaker electron density. In PDK4–AMPPNP the C-terminal residues exhibit weaker electron density, which suggests the possible presence of the cross arms. Considering

[1] Supplementary material has been deposited in the IUCr electronic archive (Reference: GX5184). Services for accessing this material are described at the back of the journal.

the observed structural deviations, it is worthwhile describing both subunits of each PDK4 dimer.

Structures of human PDK4 crystallized in the presence of ADP have been determined with and without phosphate ions (PDB entries 2zkj and 3d2r, respectively; Wynn *et al.*, 2008). These previously reported PDK4–ADP structures are essentially the same as ours, with a few notable differences. In the previous PDK4–ADP structures the C-terminal tails of the two subunits form cross arms, while in ours the C-terminal tail of subunit *A* is not clearly identified, as described above. In addition, in subunit *B* the ATP lid is more disordered and α7 adopts a different conformation, while subunit *A* assumes a similar conformation, compared with their counterparts in the previous structures (Supplementary Fig. S3). These differences may be a consequence of variations in the crystallization conditions.

3.3. PDK4 adopts a flexible open conformation

The structure of human PDK4 in complex with M77976 resembles those of human PDK3–L2 complexed with ATP (PDB entry 1y8p; Kato *et al.*, 2005) and rat PDK2–L2 complexed with AMPPNP (PDB entry 3clr; Green *et al.*, 2008) in the open conformation, rather than that of rat PDK2 complexed with ADP (PDB entry 1jm6; Steussy *et al.*, 2001) in the closed conformation (Figs. 2*a*, 2*d*, 2*e* and 2*f*). As in human PDK3–L2, the active-site cleft of the M77976-bound PDK4 is wider than that of the closed conformation of rat PDK2 (Fig. 3*a*). This result is consistent with the previous report that PDK4 by itself assumes a metastable open conformation in the absence of L2 (Wynn *et al.*, 2008). However, the inhibitor-bound PDK4 structures in this study display significant variations, as described below.

The structure of the ADP-bound PDK4 is highly superimposable on that of the AMPPNP-bound PDK4, with r.m.s.d.s of 0.4 Å for subunit *A* and 0.5 Å for subunit *B*. However, we noticed that the M77976-bound PDK4 exhibited larger r.m.s.d.s than both the AMPPNP-bound and ADP-bound PDK4s (0.9 Å for subunit *A* and 1.1 Å for subunit *B*). These structural differences primarily arise from variations in the relative arrangement of the N- and C-terminal domains in each subunit, which can be compared by superposition of the C-terminal domains (Fig. 3*b*). The active-site cleft of the ADP-bound PDK4 is slightly wider than that of the AMPPNP-bound PDK4, while that of the M77976-bound PDK4 is even wider than those of the AMPPNP-bound and ADP-bound PDK4s. These observations indicate that the domain arrangement of PDK4 is flexibly altered by the ligands bound to the ATP-binding site. The observed differences between the PDK4 structures are in contrast to the previous reports that the domain arrangement of PDK3 in complex with L2 remains unchanged upon the binding of ATP, ADP and the inhibitor radicicol (Kato *et al.*, 2005, 2007). This is probably because the L2 domain locks the PDK3 dimer in the open conformation by stabilizing the interactions between the N-terminal domain and the C-terminal tail (Figs. 2*d* and 3*a*).

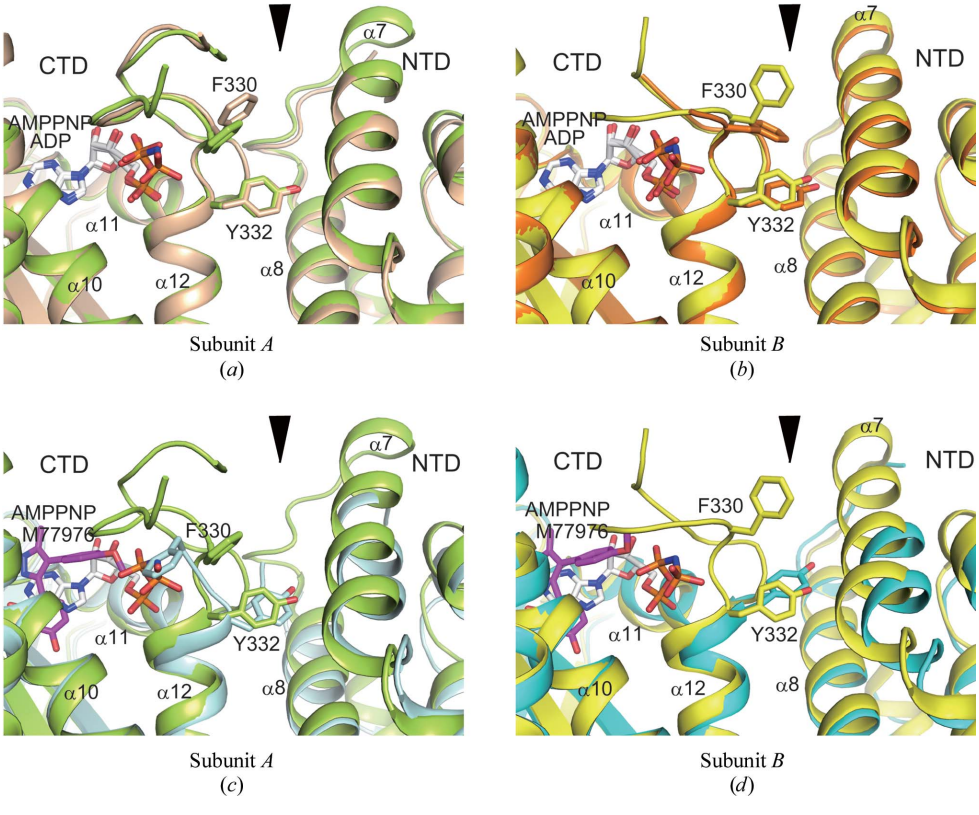

Figure 7
Superposition of the interdomain regions of (*a*, *b*) PDK4–ADP (subunit *A*, wheat; subunit *B*, orange) and (*c*, *d*) PDK4–M77976 (subunit *A*, pale cyan; subunit *B*, dark cyan) onto PDK4–AMPPNP (subunit *A*, lime green; subunit *B*, yellow) based on the C-terminal domain. NTD and CTD denote the N-terminal and C-terminal domains, respectively. The arrowhead indicates the active-site cleft.

3.4. Ligand-binding modes of PDK4

We first compared the binding modes of AMPPNP and ADP in PDK4. The γ-phosphate group of AMPPNP forms hydrogen bonds to the main-chain imino groups of Gly331, Tyr332 and Gly333 of PDK4 (Figs. 4*a* and 4*b*, red dashed lines). In addition, water-mediated hydrogen bonds exist between the γ-phosphate group and the main-chain carbonyl group of either Pro326 (subunit *A*; Fig. 4*a*) or Leu327 (subunit *B*; Fig. 4*b*) from the ATP lid. Naturally, these interactions are lost in the ADP-bound PDK4. The lack

of the γ-phosphate group interactions causes minor structural differences (Figs. 4*c* and 4*d*). Firstly, the ATP lid is more disordered compared with the AMPPNP-bound PDK4. The ATP-lid residues, such as Thr313–Pro317 and Pro326–Phe330 in subunit *A* and Gly329–Phe330 in subunit *B*, of the ADP-bound PDK4 are slightly (∼0.5 Å) more distant from the β-phosphate group than those of the AMPPNP-bound PDK4, while most of the ligand-binding residues of the ADP-bound form superpose well on those of the AMPPNP-bound form.

M77976 binds to the nucleotide-binding pocket of PDK4, occupying the position of the adenine and ribose groups of the bound AMPPNP in PDK4–AMPPNP (Figs. 5*a* and 5*b*). M77976 makes hydrophobic interactions with the side chains of Asn258, Ala262, Val298, Leu306 and Thr358 of PDK4. M77976 also forms direct or water-mediated hydrogen bonds to the side chains of Asp293 and Thr358, the main-chain carbonyl groups of Leu255, Ile291 and Thr358, and the main-chain carbonyl group of either Gly297 (subunit *A*; Fig. 5*a*) or Gly295 (subunit *B*; Fig. 5*b*). In subunit *A* Phe330 from the ATP lid exhibits additional interactions with M77976, while this residue is disordered in subunit *B*.

Compared with PDK4–AMPPNP, the ATP lid is much more disordered and residues Tyr332–Leu334 (α12) exhibit larger shifts (1.0–1.5 Å) in both subunits of PDK4–M77976 (Figs. 5*c* and 5*d*). This can be explained by the loss of the hydrogen-bonding interactions of these residues with the phosphate groups of AMPPNP. Leu306 (α11) also shifts to optimize the interaction with M77976. In addition, the side chain of Arg261, which coordinates the ribose ring of AMPPNP, moves upward to accommodate M77976. Thus, although there are some deviations between the subunits in both PDK4–M77976 and PDK4–AMPPNP, we found that the common effects of M77976 binding reside in the complete disordering of the ATP lid and the dislocation of residues from the flanking α11 and α12 helices.

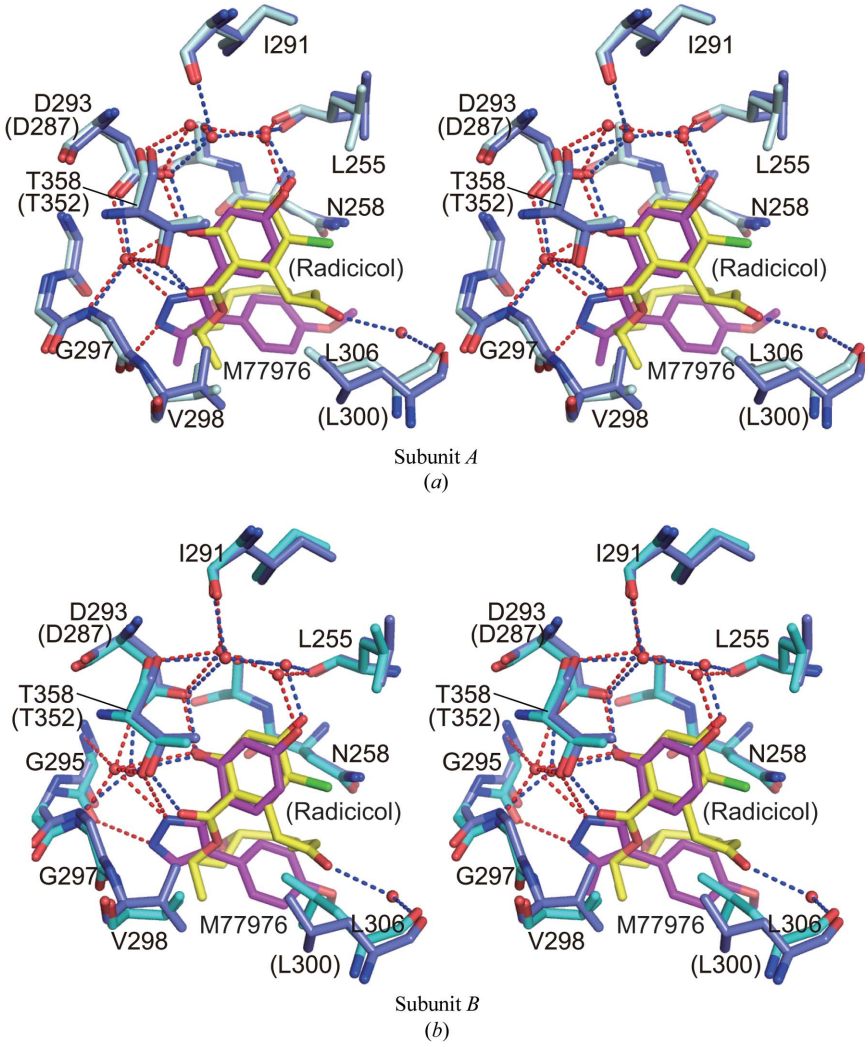

Figure 8
Interactions between PDK4 residues and M77976 in (*a*) subunit *A* and (*b*) subunit *B* in comparison with those between PDK3 residues and radicicol in PDK3–L2–radicicol (PDB entry 2q8i) (stereoview). M77976 and radicicol are shown as magenta-based and yellow-based stick models, respectively. Hydrogen bonds are shown by red (for PDK4–M77976) or blue (for PDK3–L2–radicicol) dashed lines and coordinating water molecules are indicated as dots. Labels in parentheses indicate PDK3 residue numbers.

3.5. Widening of the active-site cleft by the inhibitors

We next examined the underlying mechanism by which PDK4 alters its domain arrangement. In both subunits of PDK4–M77976, PDK4–AMPPNP and PDK4–ADP, the side chain of Tyr332 (α12) forms hydrophobic interactions with Ala135 (α7) from the N-terminal domain (Figs. 6*a*, 6*b* and 6*c*). This Tyr residue is conserved throughout the isoforms and species, and the corresponding Tyr residues exhibit similar interactions in the open conformations of the human PDK3–L2 and rat PDK2–L2 complexes (Figs. 6*d* and 6*e*). In contrast, in the closed conformation of rat PDK2 complexed with ADP the side chain of the corresponding Tyr is rotated out of the cleft because it cannot be accommodated in the narrower active-site cleft (Fig. 6*f*). Instead, the side chain of Met307 (the ATP lid) interacts hydrophobically with those of Val134 (α7) and Ile151 (α8) from the N-terminal domain. These PDK2 residues are not conserved in PDK4, and the corresponding residues, Thr310 (the ATP lid), Ile138 (α7) and Leu155 (α8), of PDK4 do not interact with each other (Figs. 6*a*, 6*b* and 6*c*). Therefore, the width of the active-site cleft of PDK4 is determined by the location of the Tyr332 side chain.

Compared with the AMPPNP-bound PDK4, α7 shifts slightly away from the C-terminal domain in the ADP-bound PDK4, according to the position of Tyr332, in both

subunits of the PDK4 dimers (Figs. 7*a* and 7*b*). Notably, in subunit *B* the side chain of Phe330 occupies the space vacated by this shift (Fig. 7*b*). On the other hand, the M77976-bound PDK4 exhibits a larger shift in α7, with greater structural differences in Tyr332 and the surrounding region in both subunits (Figs. 7*c* and 7*d*). The α11 and α12 helices shift toward the N-terminal domain, efficiently dislocating the α7 helix and expanding the active-site cleft. Therefore, in the case of PDK4, which adopts an open conformation in the absence of L2, the flexible ATP lid and the flanking regions in the C-terminal domain directly alter the relative location of the N-terminal domain.

The high-affinity binding of ADP prevents efficient ADP/ATP exchange, resulting in product inhibition by ADP. In the case of PDK3, the L2-mediated widening of the active-site cleft is related to the reduced affinity of ADP for PDK3, which is favoured for efficient release of the product ADP from the binding site (Kato *et al.*, 2005). Therefore, the slight widening of the active-site cleft in ADP-bound PDK4 compared with AMPPNP-bound PDK4 may reflect the different affinities for the bound nucleotide, although the structural comparison cannot rule out the possibility of crystal-packing effects.

3.6. Comparison with the radicicol-bound PDK3 structure

Superposition of the PDK4–M77976 and PDK3–L2–radicicol structures revealed that the dihydroxyphenyl rings of the inhibitors form a common hydrogen-bonding network with their binding residues (Figs. 8*a* and 8*b*). However, the remaining portions of the inhibitors possess different groups and exhibit different interactions. For example, the pyrazole ring of M77976 directly hydrogen bonds to the main-chain carbonyl group of PDK4 (Gly297 in subunit *A* and Gly295 in subunit *B*), but the corresponding group of radicicol lacks the equivalent interactions with PDK3. Instead, radicicol forms an indirect hydrogen bond to the main-chain carbonyl group of Leu300 of PDK3. These differences account for the slightly lower IC_{50} value of M77976 for PDK4 compared with radicicol (Fig. 1*c*).

4. Conclusions

The present data on the structures of human PDK4 have expanded our understanding of the PDK-family proteins. Significant differences were identified by comparison of the three PDK4 structures. The binding of ADP compared with AMPPNP causes a slight widening of the active-site cleft which was not detected in the previous PDK structures. Another unique feature is the geometry of the PDK4 nucleotide-binding site, which accommodates the M77976 inhibitor. Although several inhibitor-bound structures of human PDK1, PDK2 and PDK3–L2 have been determined in open conformations with a wider active-site cleft compared with the closed conformation of rat PDK2–ADP, the PDK4 structures in this study are the first to demonstrate conformational changes caused by inhibitor binding to the nucleotide-binding site. *In vitro* inhibition assays revealed that M77976 inhibits PDK4 with improved potency compared with radicicol. Thus, M77976 can be used as a lead compound for the development of more potent inhibitors targeting the nucleotide-binding pocket of PDK4.

We thank Tomomi Uchikubo-Kamo, Chiemi Mishima-Tsumagari and Toru Sengoku for technical assistance. This work was supported by the RIKEN Structural Genomics/Proteomics Initiative (RSGI), the National Project on Protein Structural and Functional Analyses, the Ministry of Education, Culture, Sports, Science and Technology of Japan.

References

Bowker-Kinley, M. M., Davis, W. I., Wu, P., Harris, R. A. & Popov, K. M. (1998). *Biochem. J.* **329**, 191–196.
Bowker-Kinley, M. & Popov, K. M. (1999). *Biochem. J.* **344**, 47–53.
Brünger, A. T., Adams, P. D., Clore, G. M., DeLano, W. L., Gros, P., Grosse-Kunstleve, R. W., Jiang, J.-S., Kuszewski, J., Nilges, M., Pannu, N. S., Read, R. J., Rice, L. M., Simonson, T. & Warren, G. L. (1998). *Acta Cryst.* D**54**, 905–921.
DeLano, W. L. (2002). *PyMOL*. http://www.pymol.org.
Dutta, R. & Inouye, M. (2000). *Trends Biochem. Sci.* **25**, 24–28.
Green, T., Grigorian, A., Klyuyeva, A., Tuganova, A., Luo, M. & Popov, K. M. (2008). *J. Biol. Chem.* **283**, 15789–15798.
Gudi, R., Bowker-Kinley, M. M., Kedishvili, N. Y., Zhao, Y. & Popov, K. M. (1995). *J. Biol. Chem.* **270**, 28989–28994.
Harris, R. A., Popov, K. M., Zhao, Y., Kedishvili, N. Y., Shimomura, Y. & Crabb, D. W. (1995). *Adv. Enzyme Regul.* **35**, 147–162.
Holm, L. & Sander, C. (1993). *J. Mol. Biol.* **233**, 123–138.
Holness, M. J. & Sugden, M. C. (2003). *Biochem. Soc. Trans.* **31**, 1143–1151.
Jones, T. A., Zou, J.-Y., Cowan, S. W. & Kjeldgaard, M. (1991). *Acta Cryst.* A**47**, 110–119.
Kato, M., Chuang, J. L., Tso, S.-C., Wynn, R. M. & Chuang, D. T. (2005). *EMBO J.* **24**, 1763–1774.
Kato, M., Li, J., Chuang, J. L. & Chuang, D. T. (2007). *Structure*, **15**, 992–1004.
Knoechel, T. R., Tucker, A. D., Robinson, C. M., Phillips, C., Taylor, W., Bungay, P. J., Kasten, S. A., Roche, T. E. & Brown, D. G. (2006). *Biochemistry*, **45**, 402–415.
Korotchkina, L. G. & Patel, M. S. (2001). *J. Biol. Chem.* **276**, 37223–37229.
Laskowski, R. A., MacArthur, M. W., Moss, D. S. & Thornton, J. M. (1993). *J. Appl. Cryst.* **26**, 283–291.
Liu, S., Baker, J. C. & Roche, T. E. (1995). *J. Biol. Chem.* **270**, 793–800.
Machius, M., Chuang, J. L., Wynn, R. M., Tomchick, D. R. & Chuang, D. T. (2001). *Proc. Natl Acad. Sci. USA*, **98**, 11218–11223.
Ono, K., Radke, G. A., Roche, T. E. & Rahmatullah, M. (1993). *J. Biol. Chem.* **268**, 26135–26143.
Otwinowski, Z. & Minor, W. (1997). *Methods Enzymol.* **276**, 307–326.
Patel, M. S. & Korotchkina, L. G. (2006). *Biochem. Soc. Trans.* **34**, 217–222.
Patel, M. S. & Roche, T. E. (1990). *FASEB J.* **4**, 3224–3233.
Popov, K. M., Kedishvili, N. Y., Zhao, Y., Shimomura, Y., Crabb, D. W. & Harris, R. A. (1993). *J. Biol. Chem.* **268**, 26602–26606.
Roche, T. E., Hiromasa, Y., Turkan, A., Gong, X., Peng, T., Yan, X., Kasten, S. A., Bao, H. & Dong, J. (2003). *Eur. J. Biochem.* **270**, 1050–1056.
Rowles, J., Scherer, S. W., Xi, T., Majer, M., Nickle, D. C., Rommens, J. M., Popov, K. M., Harris, R. A., Riebow, N. L., Xia, J., Tsui, L.-C.,

Bogardus, C. & Prochazka, M. (1996). *J. Biol. Chem.* **271**, 22376–22382.
Steussy, C. N., Popov, K. M., Bowker-Kinley, M. M., Sloan, R. B. Jr, Harris, R. A. & Hamilton, J. A. (2001). *J. Biol. Chem.* **275**, 37443–37450.
Sugden, M. C. & Holness, M. J. (2002). *Curr. Drug Targets*, **2**, 151–165.
Tuganova, A., Boulatnikov, I. & Popov, K. M. (2002). *Biochem. J.* **366**, 129–136.
Winn, M. D. *et al.* (2011). *Acta Cryst.* D**67**, 235–242.
Wu, P., Sato, J., Zhao, Y., Jaskiewicz, J., Popov, K. M. & Harris, R. A. (1998). *Biochem. J.* **329**, 197–201.
Wynn, R. M., Kato, M., Chuang, J. L., Tso, S.-C., Li, J. & Chuang, D. T. (2008). *J. Biol. Chem.* **283**, 25305–25315.